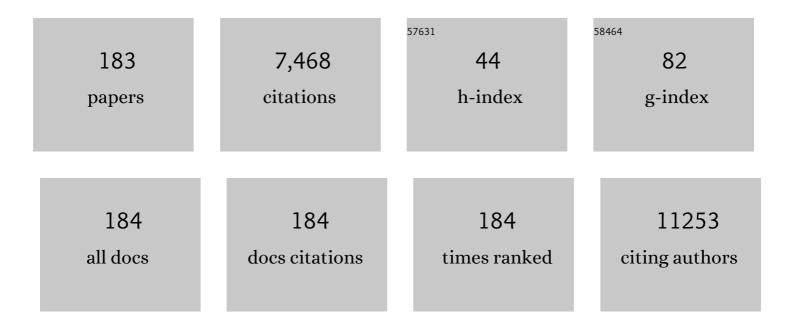
Michel Bosman

List of Publications by Year in descending order

Source: https://exaly.com/author-pdf/6567204/publications.pdf Version: 2024-02-01



#	Article	IF	CITATIONS
1	Gateâ€Defined Quantum Confinement in CVD 2D WS ₂ . Advanced Materials, 2022, 34, e2103907.	11.1	18
2	Nanoscale mapping of optically inaccessible bound-states-in-the-continuum. Light: Science and Applications, 2022, 11, 20.	7.7	28
3	Accurate and Robust Calibration of the Uniform Affine Transformation Between Scan-Camera Coordinates for Atom-Resolved In-Focus 4D-STEM Datasets. Microscopy and Microanalysis, 2022, 28, 622-632.	0.2	4
4	Spontaneous Atomic Sites Formation in Wurtzite CoO Nanorods for Robust CO ₂ Photoreduction. Advanced Functional Materials, 2022, 32, .	7.8	16
5	Coherent Sb/CuTe Core/Shell Nanostructure with Large Strain Contrast Boosting the Thermoelectric Performance of nâ€Type PbTe. Advanced Functional Materials, 2021, 31, 2007340.	7.8	30
6	Substitutional doping in 2D transition metal dichalcogenides. Nano Research, 2021, 14, 1668-1681.	5.8	92
7	Electron dynamics in plasmons. Nanoscale, 2021, 13, 2801-2810.	2.8	7
8	Controlling phase transition in WSe2 towards ideal n-type transistor. Nano Research, 2021, 14, 2703-2710.	5.8	13
9	Unlocking the origin of compositional fluctuations in InGaN light emitting diodes. Physical Review Materials, 2021, 5, .	0.9	7
10	Anomalous resistive switching in memristors based on two-dimensional palladium diselenide using heterophase grain boundaries. Nature Electronics, 2021, 4, 348-356.	13.1	112
11	Electrostatically Tunable Nearâ€Infrared Plasmonic Resonances in Solutionâ€Processed Atomically Thin NbSe ₂ . Advanced Materials, 2021, 33, e2101950.	11.1	11
12	Impurity-Induced Emission in Re-Doped WS ₂ Monolayers. Nano Letters, 2021, 21, 5293-5300.	4.5	21
13	Light-Emitting V-Pits: An Alternative Approach toward Luminescent Indium-Rich InGaN Quantum Dots. ACS Photonics, 2021, 8, 2853-2860.	3.2	10
14	A scheme for simulating multi-level phase change photonics materials. Npj Computational Materials, 2021, 7, .	3.5	27
15	Anisotropic point defects in rhenium diselenide monolayers. IScience, 2021, 24, 103456.	1.9	11
16	The nature of column boundaries in micro-structured silicon oxide nanolayers. APL Materials, 2021, 9, 121107.	2.2	2
17	Localized Probing of Dielectric Breakdown in Multilayer Hexagonal Boron Nitride. ACS Applied Materials & Interfaces, 2020, 12, 55000-55010.	4.0	11
18	Sustainable Fuel Production from Ambient Moisture via Ferroelectrically Driven MoS ₂ Nanosheets. Advanced Materials, 2020, 32, e2000971.	11.1	38

#	Article	IF	CITATIONS
19	Plasmon-Enhanced Resonant Photoemission Using Atomically Thick Dielectric Coatings. ACS Nano, 2020, 14, 8806-8815.	7.3	27
20	Sustainable Fuel Production: Sustainable Fuel Production from Ambient Moisture via Ferroelectrically Driven MoS ₂ Nanosheets (Adv. Mater. 25/2020). Advanced Materials, 2020, 32, 2070188.	11.1	2
21	Heterophase fcc-2H-fcc gold nanorods. Nature Communications, 2020, 11, 3293.	5.8	92
22	Correlation of Dielectric Breakdown and Nanoscale Adhesion in Silicon Dioxide Thin Films. , 2020, , .		2
23	Particle simulation of plasmons. Nanophotonics, 2020, 9, 3303-3313.	2.9	9
24	Revealing Electron Spill-Out in Plasmonic Nanostructures Using Particle Simulation. , 2020, , .		0
25	Particle-in-Cell Simulation of Plasmons. , 2020, , .		0
26	3D characterization of hard breakdown in RRAM device. Microelectronic Engineering, 2019, 216, 111042.	1.1	4
27	Boron Vacancies Causing Breakdown in 2D Layered Hexagonal Boron Nitride Dielectrics. IEEE Electron Device Letters, 2019, 40, 1321-1324.	2.2	16
28	Ultrasmall Designed Plasmon Resonators by Fused Colloidal Nanopatterning. ACS Applied Materials & Interfaces, 2019, 11, 45207-45213.	4.0	2
29	Giant Photoinduced Chirality in Thin Film Ge 2 Sb 2 Te 5. Physica Status Solidi - Rapid Research Letters, 2019, 13, 1900449.	1.2	2
30	Growth of Nb-Doped Monolayer WS ₂ by Liquid-Phase Precursor Mixing. ACS Nano, 2019, 13, 10768-10775.	7.3	102
31	Modeling of Diffusion and Incorporation of Interstitial Oxygen Ions at the TiN/SiO ₂ Interface. ACS Applied Materials & Interfaces, 2019, 11, 36232-36243.	4.0	9
32	An oxygen vacancy mediated Ag reduction and nucleation mechanism in SiO2 RRAM devices. Microelectronics Reliability, 2019, 98, 144-152.	0.9	16
33	Dual phases of crystalline and electronic structures in the nanocrystalline perovskite CsPbBr3. NPG Asia Materials, 2019, 11, .	3.8	41
34	Atomic Scale Modulation of Selfâ€Rectifying Resistive Switching by Interfacial Defects. Advanced Science, 2018, 5, 1800096.	5.6	29
35	Conductive Atomic Force Microscope Study of Bipolar and Threshold Resistive Switching in 2D Hexagonal Boron Nitride Films. Scientific Reports, 2018, 8, 2854.	1.6	55
36	Stochastic Modeling of FinFET Degradation Based on a Resistor Network Embedded Metropolis Monte Carlo Method. IEEE Transactions on Electron Devices, 2018, 65, 440-447.	1.6	6

#	Article	IF	CITATIONS
37	Interlayer interactions in 2D WS ₂ /MoS ₂ heterostructures monolithically grown by <i>in situ</i> physical vapor deposition. Nanoscale, 2018, 10, 22927-22936.	2.8	62
38	Photoactivity and Stability Coâ€Enhancement: When Localized Plasmons Meet Oxygen Vacancies in MgO. Small, 2018, 14, e1803233.	5.2	28
39	Theoretical Study of Ag Interactions in Amorphous Silica RRAM Devices. , 2018, , .		1
40	<i>In Situ</i> Kinetic and Thermodynamic Growth Control of Au–Pd Core–Shell Nanoparticles. Journal of the American Chemical Society, 2018, 140, 11680-11685.	6.6	66
41	Mechanism of soft and hard breakdown in hexagonal boron nitride 2D dielectrics. , 2018, , .		10
42	Ondrej Krivanek: A Research Life in EELS and Aberration Corrected STEM. Ultramicroscopy, 2017, 180, 1.	0.8	0
43	Molecular Coatings for Stabilizing Silver and Gold Nanocubes under Electron Beam Irradiation. Langmuir, 2017, 33, 1189-1196.	1.6	14
44	Textured V-Pit Green Light Emitting Diode as a Wavelength-Selective Photodetector for Fast Phosphor-Based White Light Modulation. ACS Photonics, 2017, 4, 443-448.	3.2	14
45	Intrinsic resistance switching in amorphous silicon oxide for high performance SiOx ReRAM devices. Microelectronic Engineering, 2017, 178, 98-103.	1.1	64
46	Intrinsic Resistance Switching in Amorphous Silicon Suboxides: The Role of Columnar Microstructure. Scientific Reports, 2017, 7, 9274.	1.6	41
47	Direct observation of the nanoscale Kirkendall effect during galvanic replacement reactions. Nature Communications, 2017, 8, 1224.	5.8	175
48	Statistical basis and physical evidence for clustering model in FinFET degradation. , 2017, , .		2
49	Multistep nucleation of nanocrystals in aqueous solution. Nature Chemistry, 2017, 9, 77-82.	6.6	312
50	Real-Time Dynamics of Galvanic Replacement Reactions of Silver Nanocubes and Au Studied by Liquid-Cell Transmission Electron Microscopy. ACS Nano, 2016, 10, 7689-7695.	7.3	67
51	Actively Tunable Visible Surface Plasmons in Bi ₂ Te ₃ and their Energyâ€Harvesting Applications. Advanced Materials, 2016, 28, 3138-3144.	11.1	65
52	Nanoscale Transformations in Metastable, Amorphous, Siliconâ€Rich Silica. Advanced Materials, 2016, 28, 7486-7493.	11.1	52
53	Highly Luminescent Heterostructured Copperâ€Doped Zinc Sulfide Nanocrystals for Application in Cancer Cell Labeling. ChemPhysChem, 2016, 17, 2489-2495.	1.0	17
54	Multiphysics based 3D percolation framework model for multi-stage degradation and breakdown in		2

high-Ĩº — Interfacial layer stacks. , 2016, , .

#	Article	IF	CITATIONS
55	Observation of resistive switching by physical analysis techniques. , 2016, , .		Ο
56	New understanding of dielectric breakdown in advanced FinFET devices — physical, electrical, statistical and multiphysics study. , 2016, , .		8
57	Real-Time Imaging of the Formation of Au–Ag Core–Shell Nanoparticles. Journal of the American Chemical Society, 2016, 138, 5190-5193.	6.6	55
58	Silica: Nanoscale Transformations in Metastable, Amorphous, Siliconâ€Rich Silica (Adv. Mater. 34/2016). Advanced Materials, 2016, 28, 7549-7549.	11.1	13
59	Understanding the switching mechanism in RRAM using in-situ TEM. , 2016, , .		5
60	CAFM based spectroscopy of stress-induced defects in HfO <inf>2</inf> with experimental evidence of the clustering model and metastable vacancy defect state. , 2016, , .		10
61	A plasmonic multi-logic gate platform based on sequence-specific binding of estrogen receptors and gold nanorods. Nanoscale, 2016, 8, 19973-19977.	2.8	14
62	Conductive filament formation at grain boundary locations in polycrystalline HfO2 -based MIM stacks: Computational and physical insight. Microelectronics Reliability, 2016, 64, 204-209.	0.9	12
63	Charge transfer plasmon resonances across silver–molecule–silver junctions: estimating the terahertz conductance of molecules at near-infrared frequencies. RSC Advances, 2016, 6, 70884-70894.	1.7	17
64	Room temperature stable CO _{<i>x</i>} -free H ₂ production from methanol with magnesium oxide nanophotocatalysts. Science Advances, 2016, 2, e1501425.	4.7	62
65	Compliance current dominates evolution of NiSi2 defect size in Ni/dielectric/Si RRAM devices. Microelectronics Reliability, 2016, 61, 71-77.	0.9	13
66	An experimental and theoretical investigation of the anisotropic branching in gold nanocrosses. Nanoscale, 2016, 8, 543-552.	2.8	90
67	Probabilistic insight to possibility of new metal filament nucleation during repeated cycling of conducting bridge memory. Microelectronics Reliability, 2015, 55, 1412-1416.	0.9	0
68	Evolution of Filament Formation in Ni/HfO ₂ /SiO <i>_x</i> /Siâ€Based RRAM Devices. Advanced Electronic Materials, 2015, 1, 1500130.	2.6	37
69	Nanoplasmonics in the TEM. Microscopy and Microanalysis, 2015, 21, 2219-2220.	0.2	2
70	Fast Electrical Modulation in a Plasmonicâ€Enhanced, Vâ€Pitâ€Textured, Lightâ€Emitting Diode. Advanced Optical Materials, 2015, 3, 1703-1709.	3.6	14
71	Understanding defect kinetics in ultra-thin dielectric logic and memory devices using random telegraph noise analysis. , 2015, , .		0
72	Localized Random Telegraphic Noise Study in HfO <inf>2</inf> dielectric stacks using		2

Scanning Tunneling Microscopy & amp;#x2014; Analysis of process and stress-induced traps. , 2015, , .

#	Article	IF	CITATIONS
73	Electrospun fabrication of one-dimensional composite nanofibres using colloidal gold/polymer aqueous blends. , 2015, , .		0
74	Stabilization of 4H hexagonal phase in gold nanoribbons. Nature Communications, 2015, 6, 7684.	5.8	215
75	Statistics of retention failure in the low resistance state for hafnium oxide RRAM using a Kinetic Monte Carlo approach. Microelectronics Reliability, 2015, 55, 1422-1426.	0.9	14
76	Crystallization of Sputter-Deposited Amorphous (FeSi2)1–xAlx Thin Films. Crystal Growth and Design, 2015, 15, 1692-1696.	1.4	9
77	Surface modification-induced phase transformation of hexagonal close-packed gold square sheets. Nature Communications, 2015, 6, 6571.	5.8	195
78	An SEM/STM based nanoprobing and TEM study of breakdown locations in HfO2/SiOx dielectric stacks for failure analysis. Microelectronics Reliability, 2015, 55, 1450-1455.	0.9	4
79	Spectroscopy of SILC trap locations and spatial correlation study of percolation path in the high-κ and interfacial layer. , 2015, , .		3
80	Monte Carlo model of reset stochastics and failure rate estimation of read disturb mechanism in HfO <inf>x</inf> RRAM. , 2015, , .		3
81	Visible Surface Plasmon Modes in Single Bi ₂ Te ₃ Nanoplate. Nano Letters, 2015, 15, 8331-8335.	4.5	71
82	Multimodal plasmonics in fused colloidal networks. Nature Materials, 2015, 14, 87-94.	13.3	57
83	Leakage current and structural analysis of annealed HfO2/La2O3 and CeO2/La2O3 dielectric stacks: A nanoscopic study. Journal of Vacuum Science and Technology B:Nanotechnology and Microelectronics, 2014, 32, 03D125.	0.6	4
84	A circuit model for plasmonic resonators. Optics Express, 2014, 22, 9809.	1.7	54
85	Nucleation Dynamics of Water Nanodroplets. Microscopy and Microanalysis, 2014, 20, 407-415.	0.2	19
86	An Epitaxial Ferroelectric Tunnel Junction on Silicon. Advanced Materials, 2014, 26, 7185-7189.	11.1	61
87	Spatial correlation of conductive filaments for multiple switching cycles in CBRAM. , 2014, , .		1
88	Quantum Plasmon Resonances Controlled by Molecular Tunnel Junctions. Science, 2014, 343, 1496-1499.	6.0	388
89	Au Nanoparticleâ€Modified MoS ₂ Nanosheetâ€Based Photoelectrochemical Cells for Water Splitting. Small, 2014, 10, 3537-3543.	5.2	265
90	Direct evidence of plasmon enhancement on photocatalytic hydrogen generation over Au/Pt-decorated TiO ₂ nanofibers. Nanoscale, 2014, 6, 5217-5222.	2.8	143

#	Article	IF	CITATIONS
91	Assessment of read disturb immunity in conducting bridge memory devices – A thermodynamic perspective. Microelectronics Reliability, 2014, 54, 2295-2299.	0.9	0
92	Variability model for forming process in oxygen vacancy modulated high-κ based resistive switching memory devices. Microelectronics Reliability, 2014, 54, 2266-2271.	0.9	4
93	Impact of local structural and electrical properties of grain boundaries in polycrystalline HfO2 on reliability of SiOx interfacial layer. Microelectronics Reliability, 2014, 54, 1712-1717.	0.9	11
94	Impact of ionic drift and vacancy defect passivation on TDDB statistics and lifetime enhancement of metal gate high-κ stacks. , 2014, , .		2
95	Fabrication of suspended metal–dielectric–metal plasmonic nanostructures. Nanotechnology, 2014, 25, 135303.	1.3	16
96	Edge-Gold-Coated Silver Nanoprisms: Enhanced Stability and Applications in Organic Photovoltaics and Chemical Sensing. Journal of Physical Chemistry C, 2014, 118, 12459-12468.	1.5	55
97	Water Splitting: Au Nanoparticle-Modified MoS2Nanosheet-Based Photoelectrochemical Cells for Water Splitting (Small 17/2014). Small, 2014, 10, 3536-3536.	5.2	2
98	Stochastic failure model for endurance degradation in vacancy modulated HfO <inf>x</inf> RRAM using the percolation cell framework. , 2014, , .		7
99	Encapsulated Annealing: Enhancing the Plasmon Quality Factor in Lithographically–Defined Nanostructures. Scientific Reports, 2014, 4, 5537.	1.6	96
100	Synthesis of Spiky Ag–Au Octahedral Nanoparticles and Their Tunable Optical Properties. Journal of Physical Chemistry C, 2013, 117, 16640-16649.	1.5	44
101	Multi-layered liposomes as optical resonators. , 2013, , .		1
102	Scrolling graphene into nanofluidic channels. Lab on A Chip, 2013, 13, 2874.	3.1	60
103	Electron-Energy Loss Study of Nonlocal Effects in Connected Plasmonic Nanoprisms. ACS Nano, 2013, 7, 6287-6296.	7.3	62
104	Nanoscale phase domain structure and associated device performance of organic solar cells based on a diketopyrrolopyrrole polymer. RSC Advances, 2013, 3, 20113.	1.7	15
105	Study of preferential localized degradation and breakdown of HfO2/SiOx dielectric stacks at grain boundary sites of polycrystalline HfO2 dielectrics. Microelectronic Engineering, 2013, 109, 364-369.	1.1	45
106	Impact of local variations in high-k dielectric on breakdown and recovery characteristics of advanced gate stacks. , 2013, , .		2
107	Feasibility of SILC Recovery in Sub-10-à EOT Advanced Metal Gate–High-\$kappa\$ Stacks. IEEE Electron Device Letters, 2013, 34, 1053-1055.	2.2	8
108	The "buffering" role of high-к in post breakdown degradation immunity of advanced dual layer dielectric gate stacks. , 2013, , .		6

#	Article	IF	CITATIONS
109	Intrinsic nanofilamentation in resistive switching. Journal of Applied Physics, 2013, 113, 114503.	1.1	69
110	Facile Synthesis of Luminescent AgInS ₂ –ZnS Solid Solution Nanorods. Small, 2013, 9, 2689-2695.	5.2	32
111	Fowler–Nordheim Tunneling Induced Charge Transfer Plasmons between Nearly Touching Nanoparticles. ACS Nano, 2013, 7, 707-716.	7.3	114
112	Multiferroicity in manganite/titanate superlattices determined by oxygen pressure-mediated cation defects. Journal of Applied Physics, 2013, 113, 164302.	1.1	2
113	C-Si surface passivation by aluminum oxide studied with electron energy loss spectroscopy. , 2013, , .		1
114	Surfactantâ€Free Subâ€⊋ nm Ultrathin Triangular Gold Nanoframes. Small, 2013, 9, 2880-2886.	5.2	66
115	The effect of high deposition energy of carbon overcoats on perpendicular magnetic recording media. Applied Physics Letters, 2013, 103, .	1.5	3
116	Surface Plasmon Damping Quantified with an Electron Nanoprobe. Scientific Reports, 2013, 3, 1312.	1.6	133
117	Real-time analysis of ultra-thin gate dielectric breakdown and recovery - A reality. , 2013, , .		4
118	Silicon surface passivation by aluminium oxide studied with electron energy loss spectroscopy. Physica Status Solidi - Rapid Research Letters, 2013, 7, 937-941.	1.2	29
119	Resilience of ultra-thin oxynitride films to percolative wear-out and reliability implications for high-Î ^o stacks at low voltage stress. Journal of Applied Physics, 2013, 114, 094504.	1.1	8
120	Barrier height determination of Au/Oxidized GaAs/n-GaAs using ballistic electron emission spectroscopy. Journal of Vacuum Science and Technology B:Nanotechnology and Microelectronics, 2012, 30, .	0.6	2
121	Effect of surface contamination on electron tunneling in the high bias range. Journal of Vacuum Science and Technology A: Vacuum, Surfaces and Films, 2012, 30, 041402.	0.9	3
122	Dielectric breakdown — Recovery in logic and resistive switching in memory — Bridging the gap between the two phenomena. , 2012, , .		2
123	High Hardness B _{<i>a</i>} C _{<i>b</i>} -(B _{<i>x</i>} O _{<i>y</i>} /BN) Composites with 3D Mesh-Like Fine Grain-Boundary Structure by Reactive Spark Plasma Sintering. Journal of Nanoscience and Nanotechnology. 2012. 12. 959-965.	0.9	24
124	Nanopatterning with the Helium Ion Microscope. Microscopy and Microanalysis, 2012, 18, 800-801.	0.2	1
125	Role of grain boundary percolative defects and localized trap generation on the reliability statistics of high-κ gate dielectric stacks. , 2012, , .		15
126	Spin-polarized Wide Electron Slabs in Functionally Graded Polar Oxide Heterostructures. Scientific Reports, 2012, 2, 533.	1.6	16

#	Article	IF	CITATIONS
127	Subthreshold characteristics of ballistic electron emission spectra. Journal of Applied Physics, 2012, 111, .	1.1	7
128	Nanoscale physical analysis of localized breakdown events in HfO <inf>2</inf> /SiO <inf>X</inf> dielectric stacks: A correlation study of STM induced BD with C-AFM and TEM. , 2012, , .		3
129	Light Splitting in Nanoporous Gold and Silver. ACS Nano, 2012, 6, 319-326.	7.3	44
130	Three-dimensional tubular arrays of MnO ₂ –NiO nanoflakes with high areal pseudocapacitance. Journal of Materials Chemistry, 2012, 22, 2419-2426.	6.7	408
131	Synthesis of Silver Nanoparticles with Monovalently Functionalized Self-Assembled Monolayers. Australian Journal of Chemistry, 2012, 65, 275.	0.5	13
132	The electronic barrier height of silicon native oxides at different oxidation stages. Journal of Applied Physics, 2012, 111, .	1.1	2
133	Triggering voltage for post-breakdown random telegraph noise in HfLaO dielectric metal gate metal-oxide-semiconductor field effect transistors and its reliability implications. Journal of Applied Physics, 2012, 111, 024101.	1.1	3
134	Study of charge distribution and charge loss in dual-layer metal-nanocrystal-embedded high-κ/SiO2 gate stack. Applied Physics Letters, 2012, 100, 193109.	1.5	1
135	Nanoplasmonics: Classical down to the Nanometer Scale. Nano Letters, 2012, 12, 1683-1689.	4.5	389
136	Interface and Surface Cation Stoichiometry Modified by Oxygen Vacancies in Epitaxial Manganite Films. Advanced Functional Materials, 2012, 22, 4312-4321.	7.8	65
137	Thermal conductivity of nanocrystalline carbon films studied by pulsed photothermal reflectance. Carbon, 2012, 50, 1428-1431.	5.4	19
138	Percolative Model and Thermodynamic Analysis of Oxygen-Ion-Mediated Resistive Switching. IEEE Electron Device Letters, 2012, 33, 712-714.	2.2	19
139	Colloidal Nanocrystals of Wurtziteâ€Type Cu ₂ ZnSnS ₄ : Facile Noninjection Synthesis and Formation Mechanism. Chemistry - A European Journal, 2012, 18, 3127-3131.	1.7	138
140	Gold Coating of Silver Nanoprisms. Advanced Functional Materials, 2012, 22, 849-854.	7.8	116
141	Modified Percolation Model for Polycrystalline High-\$ kappa\$ Gate Stack With Grain Boundary Defects. IEEE Electron Device Letters, 2011, 32, 78-80.	2.2	30
142	Electronic properties of ultrathin high-lº dielectrics studied by ballistic electron emission microscopy. Journal of Vacuum Science and Technology B:Nanotechnology and Microelectronics, 2011, 29, .	0.6	3
143	Very Low Reset Current for an RRAM Device Achieved in the Oxygen-Vacancy-Controlled Regime. IEEE Electron Device Letters, 2011, 32, 716-718.	2.2	27
144	Filamentation Mechanism of Resistive Switching in Fully Silicided High- \$kappa\$ Gate Stacks. IEEE Electron Device Letters, 2011, 32, 455-457.	2.2	13

#	Article	IF	CITATIONS
145	Oxygen-Soluble Gate Electrodes for Prolonged High-\$ kappa\$ Gate-Stack Reliability. IEEE Electron Device Letters, 2011, 32, 252-254.	2.2	20
146	One-Pot Synthesis of Cu _{1.94} Sâ^'CdS and Cu _{1.94} Sâ^'Zn _{<i>x</i>} Cd _{1â^'<i>x</i>} S Nanodisk Heterostructures. Journal of the American Chemical Society, 2011, 133, 2052-2055.	6.6	103
147	Annular electron energy-loss spectroscopy in the scanning transmission electron microscope. Ultramicroscopy, 2011, 111, 1540-1546.	0.8	2
148	Germanium Nanowire Metal–Oxide–Semiconductor Field-Effect Transistor Fabricated by Complementary-Metal–Oxide–Semiconductor-Compatible Process. IEEE Transactions on Electron Devices, 2011, 58, 74-79.	1.6	11
149	Ternary Cobalt–Iron Phosphide Nanocrystals with Controlled Compositions, Properties, and Morphologies from Nanorods and Nanorice to Split Nanostructures. Chemistry - A European Journal, 2011, 17, 5982-5988.	1.7	41
150	Field emission enhancement and microstructural changes of carbon films by single pulse laser irradiation. Carbon, 2011, 49, 1018-1024.	5.4	29
151	Plasma density induced formation of nanocrystals in physical vapor deposited carbon films. Carbon, 2011, 49, 1733-1744.	5.4	34
152	Physical analysis of breakdown in high-î⁰/metal gate stacks using TEM/EELS and STM for reliability enhancement (invited). Microelectronic Engineering, 2011, 88, 1365-1372.	1.1	19
153	Evidence for compliance controlled oxygen vacancy and metal filament based resistive switching mechanisms in RRAM. Microelectronic Engineering, 2011, 88, 1124-1128.	1.1	44
154	Using post-breakdown conduction study in a MIS structure to better understand the resistive switching mechanism in an MIM stack. Nanotechnology, 2011, 22, 455702.	1.3	12
155	Uncorrelated multiple conductive filament nucleation and rupture in ultra-thin high-κ dielectric based resistive random access memory. Applied Physics Letters, 2011, 99, 093502.	1.5	24
156	Threshold shift observed in resistive switching in metal-oxide-semiconductor transistors and the effect of forming gas anneal. Applied Physics Letters, 2011, 99, 232909.	1.5	4
157	Nanoscale electrical and physical study of polycrystalline high-κ dielectrics and proposed reliability enhancement techniques. , 2011, , .		4
158	Random telegraph noise reduction in metal gate high-κ stacks by bipolar switching and the performance boosting technique. , 2011, , .		3
159	Chemical insight into origin of forming-free resistive random-access memory devices. Applied Physics Letters, 2011, 99, 133504.	1.5	14
160	Grain boundary assisted degradation and breakdown study in cerium oxide gate dielectric using scanning tunneling microscopy. Applied Physics Letters, 2011, 98, 072902.	1.5	30
161	<pre>\$nhbox{-ZnO}/nhbox{-GaAs}\$ Heterostructured White Light-Emitting Diode: Nanoscale Interface Analysis and Electroluminescence Studies. IEEE Transactions on Electron Devices, 2010, 57, 129-133.</pre>	1.6	13
162	Direct visualization and in-depth physical study of metal filament formation in percolated high-κ dielectrics. Applied Physics Letters, 2010, 96, .	1.5	31

#	Article	IF	CITATIONS
163	Role of oxygen vacancies in HfO2-based gate stack breakdown. Applied Physics Letters, 2010, 96, .	1.5	41
164	Resistive switching in NiSi gate metal-oxide-semiconductor transistors. Applied Physics Letters, 2010, 97, 202904.	1.5	27
165	Localized degradation and breakdown study of cerium-oxide high-к gate dielectric material using scanning tunneling microscopy. , 2010, , .		5
166	Study of ion beam damage on FIB prepared TEM samples. , 2010, , .		6
167	The distribution of chemical elements in Al- or La-capped high-κ metal gate stacks. Applied Physics Letters, 2010, 97, 103504.	1.5	25
168	An overview of physical analysis of nanosize conductive path in ultrathin SiON and high-к gate dielectrics in nanoelectronic devices. , 2010, , .		2
169	Postbreakdown Gate-Current Low-Frequency Noise Spectrum as a Detection Tool for High- \$kappa\$ and Interfacial Layer Breakdown. IEEE Electron Device Letters, 2010, 31, 1035-1037.	2.2	5
170	New insight into the TDDB and breakdown reliability of novel high-к gate dielectric stacks. , 2010, , .		8
171	Quantitative, nanoscale mapping of sp2 percentage and crystal orientation in carbon multilayers. Carbon, 2009, 47, 94-101.	5.4	24
172	Observation of switching behaviors in post-breakdown conduction in NiSi-gated stacks. , 2009, , .		13
173	Nanoscale band gap spectroscopy on ZnO and GaN-based compounds with a monochromated electron microscope. Applied Physics Letters, 2009, 95, .	1.5	23
174	Optimizing EELS acquisition. Ultramicroscopy, 2008, 108, 837-846.	0.8	69
175	Applications and theoretical simulation of low-loss electron energy-loss spectra. Materials Science and Technology, 2008, 24, 651-659.	0.8	12
176	Theoretical interpretation of electron energy-loss spectroscopic images. AIP Conference Proceedings, 2008, , .	0.3	3
177	Plasmon resonances and electron phase shifts near Au nanospheres. Applied Physics Letters, 2008, 93, .	1.5	8
178	Simulation of Atomic Resolution Images in STEM. Microscopy and Microanalysis, 2008, 14, 922-923.	0.2	1
179	Two-Dimensional Mapping of Chemical Information at Atomic Resolution. Physical Review Letters, 2007, 99, 086102.	2.9	239
180	Mapping surface plasmons at the nanometre scale with an electron beam. Nanotechnology, 2007, 18, 165505.	1.3	256

#	Article	lF	CITATIONS
181	New developments in electron energy loss spectroscopy. Microscopy Research and Technique, 2007, 70, 211-219.	1.2	15
182	Mapping chemical and bonding information using multivariate analysis of electron energy-loss spectrum images. Ultramicroscopy, 2006, 106, 1024-1032.	0.8	261
183	Measurements of composition and electronic structure in an operating light-emitting diode using analytical electron microscopy. Applied Physics Letters, 2004, 84, 1371-1373.	1.5	3